

OnlineSI: Taming Large Language Model for Online 3D Understanding and Grounding

Zixian Liu¹, Zhaoxi Chen², Liang Pan^{3,✉}, Ziwei Liu^{2,✉}

¹Tsinghua University, ²Nanyang Technological University, ³Shanghai AI Lab

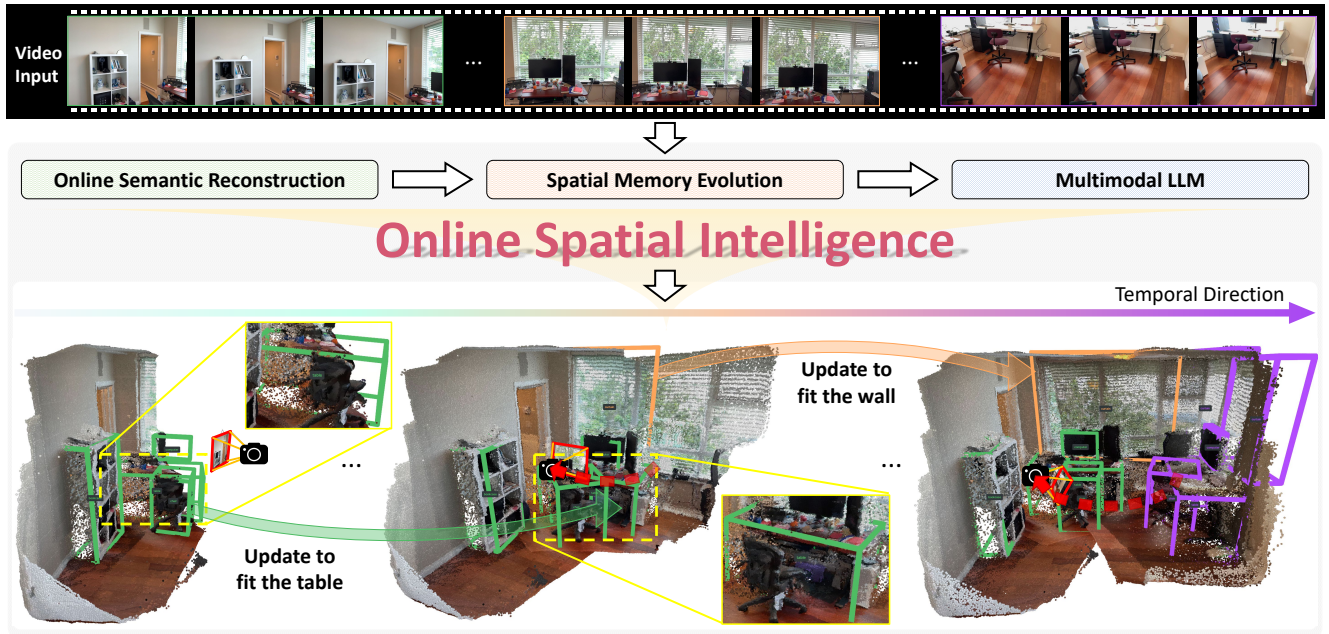


Figure 1. **OnlineSI** is a framework specifically designed for online 3D understanding and object grounding. Taking a video stream as input, **OnlineSI** performs incremental semantic reconstruction and leverages a global spatial memory to aggregate observations over time. As demonstrated in the temporal progression, this allows the framework to continuously refine its scene understanding, updating the previous detection results (e.g., “Update to fit the table”) and incrementally detecting new object instances.

Abstract

In recent years, researchers have increasingly been interested in how to enable Multimodal Large Language Models (MLLM) to possess spatial understanding and reasoning capabilities. However, most existing methods overlook the importance of the ability to continuously work in an ever-changing world, and lack the possibility of deployment on embodied systems in real-world environments. In this work, we introduce **OnlineSI**, a framework that can continuously improve its spatial understanding of its surroundings given a video stream. Our core idea is to maintain a finite spatial memory to retain past observations, ensuring the computation required for each inference does not increase as the input accumulates. We further integrate 3D point cloud information with semantic information, helping MLLM to bet-

ter locate and identify objects in the scene. To evaluate our method, we introduce the Fuzzy F_1 -Score to mitigate ambiguity, and test our method on two representative datasets. Experiments demonstrate the effectiveness of our method, paving the way towards real-world embodied systems. The project page is available at <https://onlinesi.github.io/>.

1. Introduction

Processing and understanding streaming information is crucial for embodied systems. As robotic agents move from constrained, fixed environments to dynamic, open-world scenes, and as they transition from executing short, simple skills to solving long-horizon tasks, they must be able to continuously learn from an ever-changing 3D world.

For instance, an autonomous agent exploring a novel environment must constantly update its spatial understanding from new observations and respond on the fly. Such online learning capability is a fundamental prerequisite for downstream tasks such as active learning, long-term planning, and human-robot interaction.

However, equipping Multimodal Large Language Models (MLLM) with this form of online spatial intelligence remains challenging. First, most existing methods face prohibitive computational scaling as input stream grows. The architectures that repeatedly process all past observations with full attention layers quickly exhaust the model context and computational budget due to spatial and contextual redundancy. Second, many models still fail in understanding spatial relationships and reasoning in space, a limitation that is further exacerbated by the scarcity of 3D-grounded training data. While recent works, e.g., Hu et al. [20], have explored memory management for embodied planning, their solutions have two key limitations. As task execution proceeds, the memory bank infinitely grows, leading to computational and storage bottlenecks. Furthermore, their model perceives 3D space at a coarse-grained level, rendering them unsuitable for guiding fine-grained operations such as precise object manipulation. These difficulties motivate our core research question: *Can multimodal large language models perceive and understand the 3D world in an online fashion?*

In this paper, we propose **OnlineSI**, a framework designed to understand 3D scenes in an online fashion and make detections on the fly from streaming video. Our key insight is to maintain a finite, explicit spatial memory, and leverage the multimodal model to reason over this compact memory representation for precise, object-level predictions. This design ensures a fixed upper bound for the computational budget of each inference step, effectively decoupling inference cost from the stream length. At the same time, the explicit spatial memory structure also facilitates the model’s grasp of fine-grained spatial concepts. Furthermore, we introduce a novel fusion technique that tightly integrates 3D point cloud data with semantic information, providing the MLLM with a rich, object-level understanding of the scene.

Specifically, for each incoming frame, OnlineSI leverages off-the-shelf models to extract 3D and semantic information, integrating these observations into its global spatial memory. The MLLM then processes this updated memory to output a scene description, including detection results for objects observed. As the scene is progressively reconstructed, the model not only identifies new objects but also automatically refines previous detections that were made under partial observations, as illustrated in Fig. 1.

Evaluating performance on an arbitrary video stream introduces a significant ambiguity: given the inherently incomplete observation, should a partially viewed object be

counted as a detection? To address this evaluation challenge, we propose the Fuzzy F_1 -Score, a modification of the standard F_1 -Score designed for this online, partial observation setting. We conduct extensive experiments on two representative datasets, ScanNet [10] and ScanNet++ [58]. Experimental results show that our method significantly outperforms existing baselines, demonstrate its effectiveness in the online setting.

In summary, our contributions are as follows:

- We introduce OnlineSI, a novel framework for online 3D scene understanding and grounding that maintains bounded inference costs, enabling it to process video streams incrementally.
- We propose a new fusion method that integrates 3D point cloud and semantic information, enhancing the MLLM’s object-level spatial understanding.
- We propose the Fuzzy F_1 -Score, a new evaluation metric to fairly assess detection performance under the ambiguity of partial observation, and validate our framework’s superior performance through extensive experiments.

2. Related Work

3D Object Detection aims to predict category labels and oriented 3D bounding boxes for each instance in the scene. Previous work can be divided into two main genres: methods that operate directly on 3D point clouds and those that use single-view 2D images. In the point-cloud-based genre, research has focused on enhancing the model’s understanding by enriching the 3D representation. A prominent strategy is to leverage knowledge from other modalities. For instance, [4, 5, 36, 37] tap into knowledge priors from 2D images to achieve open-vocabulary 3D detection. Similarly, [40] employs a Large Language Model (LLM) to better process global-local information. Other approaches improve the model architecture or training strategy. For example, [46] uses a vertex relative positional encoding method to help the model focus on points near objects, while [26] improves the system’s generalization through multi-dataset training. In the single-view-image-based genre, [3] pioneers unified monocular 3D object detection by training on the extensive Omni3D dataset. Following this, [31] introduces the first successful BEV-based monocular 3D object detector. A central theme in this area is addressing the scarcity of 3D training data by leveraging abundant 2D data. To this end, [21] uses open-vocabulary 2D models and pseudo-LiDAR to automatically label 3D objects. [57] leverages 2D results from Grounding DINO [34] with a 3D head to predict 3D bounding boxes. Both [24] and [60] also address data scarcity by generating pseudo-3D data from 2D annotations or leveraging pre-trained 2D model knowledge. In our work, we emphasize on online detection from a video stream. A work with similar topic is [63], which unifies grounding and exploration for embodied navigation.

Compared to their work, we train a large language model to directly understand 3D point clouds and output 3D bounding boxes with rotations and class labels.

Multimodal Large Language Models aim to understand, reason, and generate from multimodal information. Early methods, such as [42], unifies images and texts by learning a joint image-text representation. More recently, with the remarkable success of Large Language Model and scaling laws, innumerable works have been devoted to unify vision and language within a single large transformer-based model [1, 2, 8, 12, 13, 28, 29, 33, 52]. Meanwhile, others have attempted to unify multiple modalities, enabling models to understand diverse information sources [23, 25, 53]. With the rapid development of autonomous driving and embodied AI, 3D understanding has recently become a significant focus for MLLM researchers. Some works aim to enable models to perceive spatial relationships from images by training on datasets containing 3D annotations [7, 9, 38, 55], while others seek to adapt models to 3D representations for spatial reasoning [14, 16, 20, 22, 41, 50, 54, 61, 62]. However, most of the previous methods suffer from computational overload as the number of input images increases, making them unsuitable for deployment in embodied systems that need to learn at test time. Although some work has explored how to maintain a spatial memory for scene understanding [56, 64], they do not focus on continuously improving understanding and online responding. In this sense, the work most similar to ours is [20]. However, they still have problems such as memory bank growing and coarse-level understanding. In our work, we update an explicit spatial memory based on input frames and use this memory as input to the MLLM, which guarantees a bounded inference time and fine-grained understanding.

2D Object Detection is one of the most fundamental and challenging problems in computer vision. In earlier years, researchers typically use carefully designed, handcrafted features for detection [11, 15, 48]. Then with the rise of deep convolutional neural networks (CNN), many works introduced deep learning to this field, and they can be divided into two groups. The first one follows a “coarse-to-fine” process, proposing coarse regions and then focusing on them [17, 19, 44]. The second group, in contrast, retrieves all objects in one-step inference [6, 27, 32, 35, 43]. Recently, significant research has focused on open-vocabulary object detection, often achieved through large-scale pre-training [18, 30, 34, 59]. In our work, we use an off-the-shelf open-vocabulary detector to obtain pixel-level semantic labels. This semantic information is then injected into the point cloud to enhance its representation.

3. Preliminaries: SpatialLM

We leverage SpatialLM’s [39] ability of understanding point clouds to achieve online spatial intelligence. SpatialLM

is a multimodal large language model designed to understand 3D indoor environment and generate structured scene descriptions. The model employs Sonata [51] as its point cloud encoder and finetunes Llama-3.2-1B-Instruct [47] on a synthetic dataset consisting of 12,328 distinct scenes.

Given the point cloud \mathbf{P} of N points, Sonata first encodes it into 3D feature patches \mathbf{F} :

$$\mathbf{F} = \mathcal{E}(\mathbf{P}) \quad \mathbf{P} \in \mathbb{R}^{N \times 6}, \quad \mathbf{F} \in \mathbb{R}^{K \times D}, \quad (1)$$

where K is the number of feature patches and D is the feature dimension, and each point is represented by coordinates XYZ and color RGB. Then, the feature patches \mathbf{F} , along with the prompt tokens, are fed into the large language model backbone, and generate a scene description as text. This output can be subsequently interpreted as a set of 3D bounding boxes for objects in the scene.

It is worth noting that the original SpatialLM model requires the input point cloud to be aligned with the coordinate axes, i.e. the floor must be perpendicular to the z-axis and the walls must be parallel to the x and y-axis. Furthermore, the predicted 3D bounding boxes are constrained to rotations only around the z-axis. This axis-alignment constraint significantly hinders its application in the online detection, where the camera may have an arbitrary 6D pose.

4. Method

We first provide the problem formulation. Then we describe how we maintain the spatial memory from the input frames, and process it using a multimodal large language model. Subsequently, we present the design of the point cloud encoder and the semantic encoder, detailing how semantic information is injected into the point cloud features. Lastly, we introduce the Fuzzy F_1 -Score, a metric adapted for the online setting. The overview of our framework is demonstrated in Fig. 2.

4.1. Problem Formulation

Given a potentially infinite sequence of images $\{\mathbf{I}_t \in \mathbb{R}^{H \times W \times 3}\}_{t=1}^N$, for each current image \mathbf{I}_t , our goal is to predict the 3D bounding boxes and class labels for objects that have appeared in the scene, represented in a unified coordinate frame. As the system must be capable of long-term learning from the environment, we impose two constraints: the inference computational budget per frame must be capped, and the large language model’s input must not exceed its context limit. Therefore, we need to dynamically maintain a memory \mathbf{M}_t of past observations, subject to an upper bound on its size.

The multimodal large language model cannot handle point clouds with 3D rotation. Consequently, we define

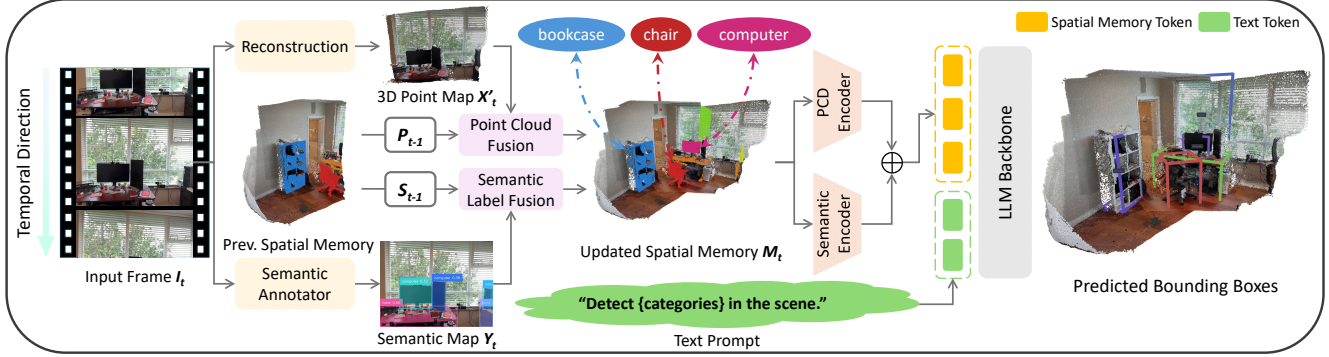


Figure 2. Overview of OnlineSI. For each frame \mathbf{I}_t in the video stream, we first reconstruct the pointmap \mathbf{X}'_t , and predict the semantic label for each point \mathbf{Y}_t . Next, we fuse the current pointmap and semantic map into the previous spatial memory $\{\mathbf{P}_{t-1}, \mathbf{S}_{t-1}\}$ for updating. We then use the point cloud encoder and the semantic encoder to obtain point cloud features and semantic features, respectively, and add them together as our spatial memory tokens. Lastly, we feed the spatial memory tokens and the text prompt tokens into the LLM backbone, and generate a scene description, which contains the detection results of objects in the current scene.

a unified coordinate frame that deviates from the convention used in 3D reconstruction tasks (i.e., the initial camera frame). Instead, our system’s origin is at the initial camera’s position, but its xy plane is parallel to the ground in the scene and its z -axis is perpendicular to it. This coordinate frame is suitable for most embodied agents, where either the camera is looking straight ahead, or we know the camera’s relative pose in the world frame. We assume the transformation from the initial camera frame to our unified, aligned coordinate frame is known, which can be derived from the camera’s pitch and roll angles. The impact of this coordinate system choice on the final performance is discussed in Sec. 5.4.

4.2. Spatial Memory Management

We chose to use explicit 3D point clouds to store past observations. The spatial memory \mathbf{M}_t consists of a point cloud part and a semantic part: $\mathbf{M}_t = \{\mathbf{P}_t, \mathbf{S}_t\}$, where $\mathbf{P}_t \in \mathbb{R}^{N \times 6}$ is the constructed point cloud and $\mathbf{S}_t \in \mathbb{Z}^N$ is the semantic label of each point. For each frame \mathbf{I}_t , we first leverage pre-trained reconstruction model to predict the pointmap $\mathbf{X}_t \in \mathbb{R}^{H \times W \times 3}$ in the initial camera frame, and obtain a semantic map $\mathbf{Y}_t \in \mathbb{Z}^{H \times W}$ through an off-the-shelf semantic annotator, where each pixel in \mathbf{Y} represents the semantic label of corresponding point in \mathbf{X}_t . The points in \mathbf{X}_t are then transformed into the unified aligned coordinate frame, yielding \mathbf{X}'_t . Subsequently, we fuse $\mathbf{X}'_t, \mathbf{Y}_t$ into the previous spatial memory:

$$\mathbf{P}_t = \text{Fuse}(\mathbf{P}_{t-1}, \mathbf{X}'_t, t), \quad \mathbf{S}_t = \text{Fuse}(\mathbf{S}_{t-1}, \mathbf{Y}_t, t), \quad (2)$$

where $\mathbf{P}_{t-1}, \mathbf{X}'_t, \mathbf{S}_{t-1}, \mathbf{Y}_t$ are sampled at specific ratios and then concatenated for updating. The sample indices are unified to ensure that points and their semantic labels correspond. To maintain \mathbf{M}_t at a fixed size and prevent forgetting of early observations as input accumulates, we adjust the fusion ratios based on the timestep t . This ensures the

total number of points in \mathbf{M}_t remains below a predefined threshold, and the number of points sampled from each input frame is uniform.

With the updated spatial memory, we use the point cloud encoder and the semantic encoder to extract point cloud features and semantic features, respectively. We then add them together to create the spatial memory tokens. After that, these spatial memory tokens, along with language instruction tokens, are fed into the large language model to generate a scene description, which contains the 3D bounding boxes of all objects detected thus far in the scene.

4.3. Point Cloud Encoder and Semantic Encoder

Large-scale pre-training enables SpatialLM to understand various indoor environments. However, we observed that SpatialLM’s performance degrades significantly when processing partially reconstructed scenes compared to full scene inputs. Therefore, we inject additional semantic information, predicted by pre-trained models, into the point cloud to aid the model in localizing and recognizing objects.

In our framework, the point cloud encoder follows the design of Sonata [51]. The point cloud \mathbf{P} is encoded into 3D feature patches \mathbf{F} , where each patch represents a cubic region. To preserve the locality of point cloud features, our semantic encoder is designed with an identical pooling structure to the point cloud encoder, but it contains no trainable parameters between pooling operations, and only passes through a final linear projection layer for fine-tuning.

Specifically, for the semantic label of each point, we first convert it to its corresponding Llama-3.2-1B-Instruct [47] token feature. We then use the same pooling operations as the point cloud encoder to aggregate these per-point features into semantic feature patches. After that, we feed the patches into a linear projection layer, and add the resulting features to the point cloud features. This design not only ensures that the semantic information and point cloud fea-

tures share the same granularity and spatial location, but also minimizes the number of trainable parameters, making fine-tuning possible even with limited 3D datasets.

4.4. Fuzzy F_1 -Score

Previous 3D bounding box detection works mostly use Mean Average Precision or F_1 Score as standard performance metrics. However, with monocular image inputs, occlusions and limited fields of view make it difficult to determine whether an object “should be detected”. This ambiguity is particularly evident in the online setting, where the camera view can change drastically. For example, if only one leg of a table is visible, the model clearly lacks sufficient information to predict its full dimensions. Conversely, a partially occluded chair in the center of the image should still be detectable.

We propose using Fuzzy F_1 -Score to mitigate the impact of this ambiguity on the final metrics. Specifically, during evaluation, we define two types of 3D bounding box annotations: the strict ground truth $O_{\text{gt}}^s = \{o_{i,\text{gt}}^s \in \mathbb{R}^7\}_{i=0}^N$ and the lenient ground truth $O_{\text{gt}}^l = \{o_{j,\text{gt}}^l \in \mathbb{R}^7\}_{j=0}^M$, where we use the position of the center, the three dimensions and z-axis rotation to represent a box. The strict ground truth is composed of objects in the lenient ground truth that have a higher visible proportion, hence we have $O_{\text{gt}}^s \subseteq O_{\text{gt}}^l$. These two sets form the lower and upper bounds, respectively, of objects the model is expected to detect. Given the model’s predictions O_{pred} , we calculate the F_1 score using the recall on O_{gt}^s and the precision on O_{gt}^l . In other words, let $\text{recall}(O_{\text{pred}}, O_{\text{gt}}^s)$ be the recall of O_{pred} over O_{gt}^s , and $\text{precision}(O_{\text{pred}}, O_{\text{gt}}^l)$ be the precision of O_{pred} over O_{gt}^l , we define:

$$\text{Fuzzy-}F_1 = 2 \cdot \frac{\text{recall}(O_{\text{pred}}, O_{\text{gt}}^s) \cdot \text{precision}(O_{\text{pred}}, O_{\text{gt}}^l)}{\text{recall}(O_{\text{pred}}, O_{\text{gt}}^s) + \text{precision}(O_{\text{pred}}, O_{\text{gt}}^l)}, \quad (3)$$

The Fuzzy F_1 -Score is thus unaffected if the model does not detect some objects with low visibility, thereby alleviates the ambiguity problem. For further details on the Fuzzy F_1 -Score, please refer to Sec. 5.4.

5. Experiments

The primary goal of our experiments is to evaluate our system’s ability to continuously build and refine its understanding of novel environments from a monocular video stream. We aim to answer the following research questions: (1) How effectively does our online system perform in novel scenes? (2) Is maintaining a persistent spatial memory superior to simply merging independent per-frame predictions? (3) How does the integration of semantic information contribute to overall performance? (4) What is the performance impact of the external modules used in our system?

In this section, we first introduce the implementation details, baselines and datasets. We then present a comprehensive comparison, including both quantitative and qualitative results, to demonstrate the effectiveness of our method. Finally, we present ablation studies, to analyze some key design choices of our method.

5.1. Experimental Setup

Implementation Details In our system, we choose CUT3R [49] as our reconstruction module, and Grounded SAM [45] as our semantic annotator. For the point cloud encoder and the LLM backbone, we initialize them with SpatialLM1.1-Llama-1B [39]. During training, we only set the last layer of the point cloud encoder and the semantic encoder, as well as the LLM backbone as trainable, keeping all other parameters frozen. Training is conducted on 8 NVIDIA A800 GPUs, using standard cross-entropy loss for language model training.

Baselines We compare our system against a series of baselines:

- **SpatialLM-No-Finetune** We directly feed the reconstructed point cloud into the original SpatialLM model without any training.
- **SpatialLM-Merge** We treat this online process as per-frame prediction. For each frame, we feed the pointmap into SpatialLM to obtain a prediction, then we merge all the detection results to obtain the current results.
- **SpatialLM-Finetune** We maintain the point cloud in the spatial memory but omit the semantic component, leveraging only the point cloud encoder to generate spatial memory tokens.
- **SpatialLM-Ground-Truth-PCD** Identical to SpatialLM-Finetune, but we use ground-truth point clouds instead of reconstructed ones.
- **SpatialLM-Ground-Truth** Identical to our method, but we use ground-truth point clouds and semantic labels.

SpatialLM-Ground-Truth-PCD and SpatialLM-Ground-Truth serve as upper-bound benchmarks, illustrating the system’s potential performance independent of errors from external modules. Comparisons with the other lower-bound baselines validate the effectiveness of our system’s specific design components.

Datasets We use ScanNet [10] and ScanNet++ [58] to benchmark our method and baselines. For bounding box annotations, we filter out small objects with all dimensions smaller than 15cm. We define object visibility as the proportion of its visible faces in a given frame and apply different visibility thresholds to filter annotations for training and evaluation. We randomly sample 1~32 frames with a stride of 30 for each sample sequence.

Method	Avg. Fuzzy- F_1	Chair	Table	Computer	Sink	Bed	Sofa	Toilet
ScanNet++								
SpatialLM-Ground-Truth-PCD	0.5708	0.7538	0.6160	0.3464	0.4078	0.8274	0.3883	0.5563
SpatialLM-Ground-Truth	0.6420	0.7541	0.6318	0.4540	0.6247	0.8263	0.4794	0.7233
SpatialLM-No-Finetune	0.0351	0.2126	0.0000	0.0194	0.0183	0.0823	0.0352	0.0559
SpatialLM-Merge	0.3397	0.5357	0.4606	0.1669	0.2320	0.4509	0.0273	0.3583
SpatialLM-Finetune	0.3943	0.5732	0.5160	0.2036	0.1451	0.4859	0.2897	0.2812
Ours	0.4397	0.6213	0.4717	0.2644	0.1683	0.6094	0.4633	0.4007
ScanNet								
SpatialLM-Ground-Truth-PCD	0.5182	0.6050	0.5254	0.1464	0.4511	0.7482	0.6855	0.8803
SpatialLM-Ground-Truth	0.6138	0.6497	0.6123	0.3059	0.6063	0.9046	0.7113	0.9442
SpatialLM-No-Finetune	0.0383	0.1291	0.0000	0.0147	0.0470	0.1708	0.1089	0.1634
SpatialLM-Merge	0.2214	0.3267	0.2237	0.1125	0.1964	0.3517	0.3159	0.3065
SpatialLM-Finetune	0.2733	0.2900	0.2893	0.1322	0.2410	0.4743	0.3666	0.5651
Ours	0.3349	0.3425	0.3287	0.1621	0.2712	0.7166	0.4395	0.6198

Table 1. **Quantitative Results of Our Experiments.** We evaluate the methods on ScanNet [10] and ScanNet++ [58]. For each method, we report the average fuzzy F_1 -score, as well as the fuzzy F_1 -scores of 7 representative categories. Our method achieves state-of-the-art performance among the non-ground-truth baselines.

5.2. Quantitative Results

As shown in Tab. 1, our method significantly outperforms the three lower-bound baselines on two benchmarks. The two upper-bound baselines, which use ground-truth data, establish the potential performance limit of our approach. This result demonstrates the overall effectiveness of our method. Furthermore, our system’s superior performance against SpatialLM-Merge highlights the importance of spatial memory maintaining, while the comparison with SpatialLM-Finetune confirms the benefits of injecting semantic information for object localization and recognition.

5.3. Qualitative Results

We compare the prediction results of our method against the three lowe-bound baselines in Fig. 3. It is evident that the original SpatialLM model (SpatialLM-No-Finetune) performs poorly when fed an online reconstructed point cloud, which is inherently partial and incomplete. Due to the incomplete information in each single-frame prediction, the merged result from SpatialLM-Merge often retains a large number of erroneous predictions. SpatialLM-Finetune often produces incorrect detections due to imperfections in the reconstructed point cloud. In contrast, our method successfully leverages its spatial memory to aggregate information over time and uses semantic cues to assist the model in locating and recognizing objects, enabling the system to build a continuous and accurate understanding of its surroundings in real-world scenes.

5.4. Ablation Study

Choice of Spatial Memory CUT3R [49] maintains a latent state representation to store the information about the current 3D scene, and the representation in the header before the output pointmap also contains 3D information. Here, we conduct ablation experiments to determine the most suitable spatial memory representation. For these two 1D memory representations we use 5 layers of cross-attention to convert them into memory tokens that are fed into LLM. The results are shown in Tab. 2. As demonstrated in the results, implicit, one-dimensional memory representations are far less effective than using an explicit three-dimensional point cloud as memory. One possible reason is that the amount of data in ScanNet++ is insufficient for training LLM to interpret these implicit representations.

Coordinate System Selection Sec. 4.1 has demonstrated the importance of choosing correct point cloud coordinate

Memory Representation	Avg. Fuzzy- F_1
1D State	0.0764
1D State + Pointmap Feats	0.0591
SpatialLM-Fintune	0.3943

Table 2. **Ablation on the Choice of Spatial Memory.** “1D State” means using the latent state representation of CUT3R [49] as the memory, “1D State + Pointmap Feats” means using both the latent state and features in the pointmap output header to obtain memory tokens. Apart from the memory, these two baselines are the same as SpaitalLM-Finetune settings. We conduct experiments on ScanNet++ [58] and report the average fuzzy F_1 -scores.

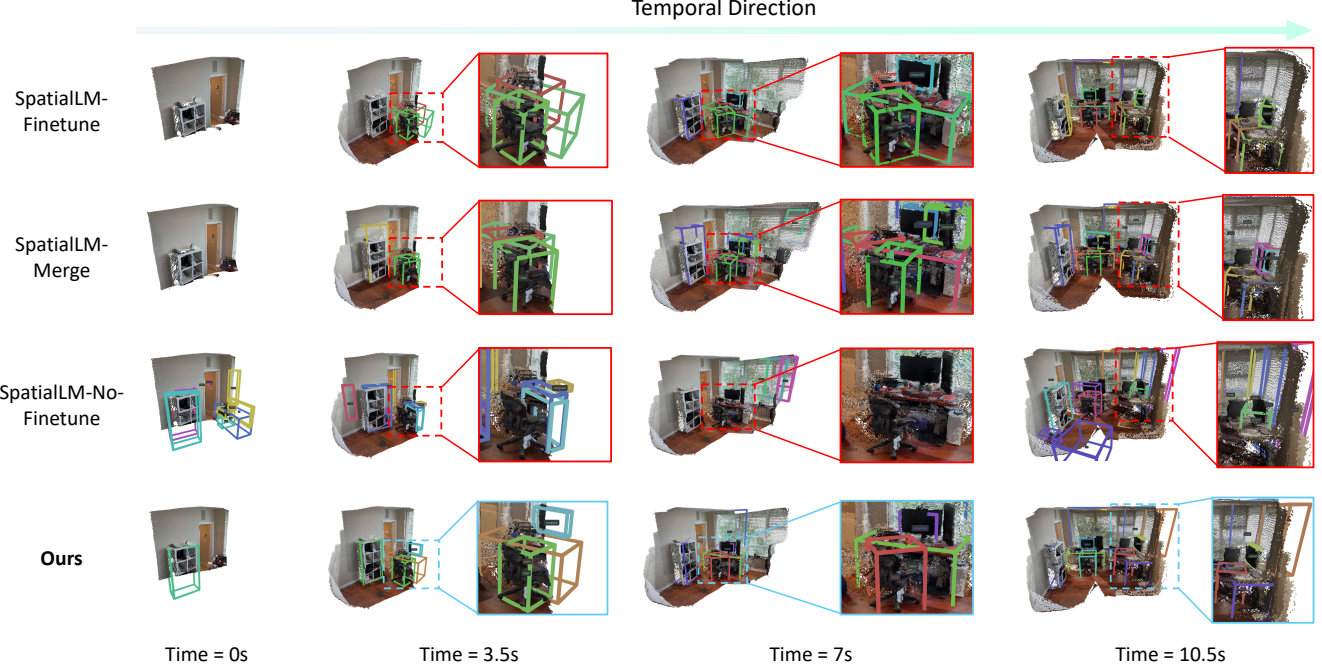


Figure 3. **Qualitative Results of the Detections.** Here we show examples comparing our method with baselines. We show the progress of scene reconstruction as input frames accumulate, and the detection results at each timestep. We zoom in on key parts of the scene to provide a clearer, more direct comparison.

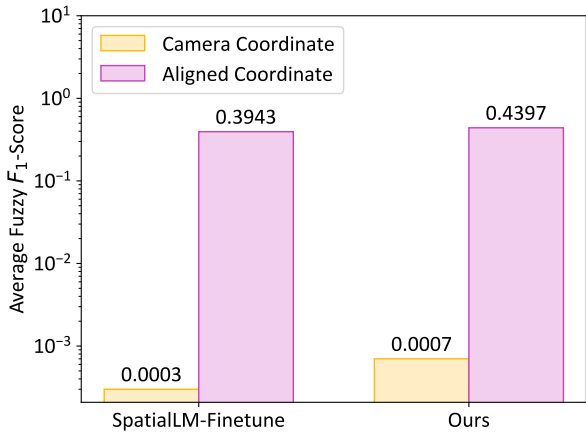


Figure 4. **Ablation on Coordinate System Selection.** We demonstrate the impact of different coordinate systems of the reconstructed point clouds on performance. We report fuzzy F_1 -scores evaluated on ScanNet++ [58].

frame. Here we use ablation experiments to quantify the impact of coordinate system selection. As shown in Fig. 4, when we use the initial camera’s coordinate frame instead of aligning it with the ground plane, the LLM largely fails to understand the input point cloud. Both our method and SpatialLM-Finetune show a significant drop in performance. This indicates that SpatialLM is incapable of understanding point clouds with arbitrary 3D rotation and can only effectively understand point clouds where the ground

plane is aligned, which means the ground plane of the point cloud is parallel to the xy plane of the coordinate frame.

Fuzzy F_1 -Score Fig. 5 provides some illustrative examples of how our fuzzy F_1 -score works. **1.** For the vanilla F_1 -Score, the final value is greatly affected by different ground truth annotations (see the middle two columns). However, due to partial obstruction, it is difficult to determine, through deterministic procedures, which objects should be detected and used as validating annotation. **2.** In our Fuzzy F_1 -Score examples on the last column, we let objects with high visibility form O_{gt}^s , and combine them with low-visibility objects to form O_{gt}^l (refer to the definition in Sec 4.4). Objects in O_{gt}^s should be detected, while objects in O_{gt}^l but not in O_{gt}^s are in an ambiguous state: not detecting them won’t affect the final result, correct detection will improve precision, while incorrect detection will decrease precision. This evaluation method ensures that objects which are at the critical point of “should be detected” do not affect the final metrics, thus mitigating the ambiguity problem in the online settings.

Semantic Representation In Sec. 4.3 we convert the semantic labels to Llama-3.2-1B-Instruct [47] token features for semantic information injection. Here we explore the effect of different semantic representation choices. We replace the Llama features to the CLIP [42] features encoded from the same texts in our method, and show the experiments results in Tab. 3. As demonstrated in the results, us-

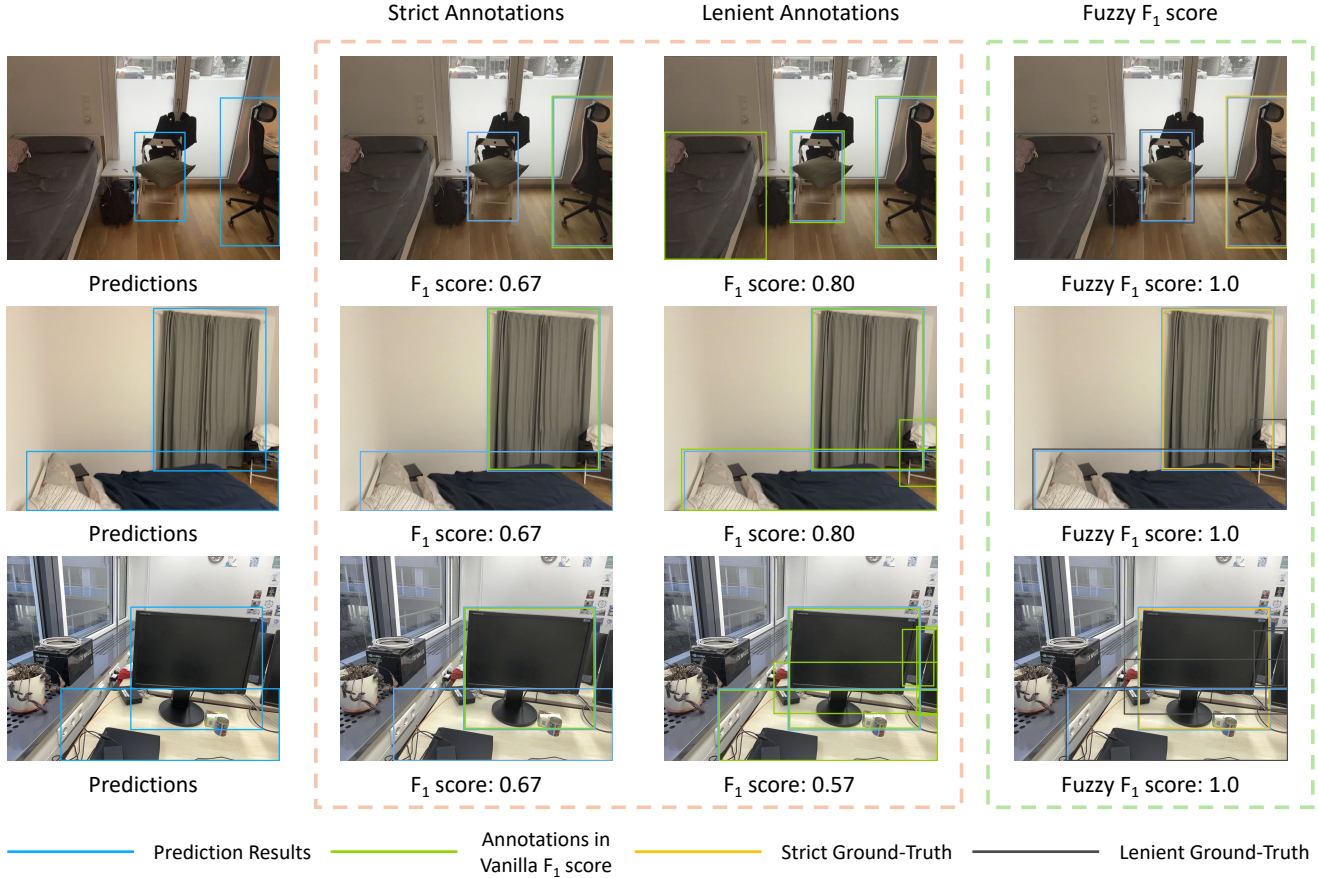


Figure 5. **Examples of Fuzzy F_1 -Score.** For each row we show the model’s [prediction](#) in the blue boxes. In the second column, we only select objects with high visibility as the evaluation [annotation](#), while in the third column, we include all low-visibility objects. The vanilla F_1 -score differs significantly between the two cases. In the last column, we present a visualization of the Fuzzy F_1 -Score. The [strict ground-truth \(must be detected\)](#) and the [lenient ground-truth \(may be detected\)](#) form the lower and upper bounds of the annotation, providing a more reasonable metrics for evaluation.

Semantic Representation	Avg. Fuzzy- F_1
CLIP	0.4319
Llama	0.4397

Table 3. **Ablation on the Semantic Representation.** We experiment with different semantic representations in the semantic encoder. All other settings are the same as our method. We report fuzzy F_1 -scores evaluated on ScanNet++ [58].

ing the same semantic representation as the LLM backbone (Llama) is slightly better than using different semantic representation (CLIP).

6. Conclusion

In this work, we introduce a novel framework for online 3D understanding and object grounding. By maintaining a finite spatial memory, our framework can continuously improve its understanding of the environment through the video stream and perform detections on the fly. Further-

more, we integrate 3D point cloud data with semantic information, demonstrate how multimodal large language models can understand 3D scenes at a more granular level. To mitigate the ambiguity problem in the online detection, we propose the Fuzzy F_1 -Score as performance metrics. Experiments demonstrate the effectiveness of our framework.

Limitations Despite these contributions, several limitations remain. First, since SpatialLM was pre-trained exclusively on indoor scene datasets, our framework’s applicability is currently restricted to similar environments. Enhancing the base model with more diverse 3D data could address this limitation. Second, we currently use a “sample and then concatenate” method to maintain the spatial memory, which poses challenges for handling dynamic scenarios. Exploring 4D reconstruction with tracking information to build the spatial memory is an interesting direction. We hope our work could inspire more future work on building spatial intelligence for real-world applications.

References

[1] Jean-Baptiste Alayrac, Jeff Donahue, Pauline Luc, Antoine Miech, Iain Barr, Yana Hasson, Karel Lenc, Arthur Mensch, Katherine Millican, Malcolm Reynolds, et al. Flamingo: a visual language model for few-shot learning. *Advances in neural information processing systems*, 35:23716–23736, 2022. 3

[2] Shuai Bai, Keqin Chen, Xuejing Liu, Jialin Wang, Wenbin Ge, Sibo Song, Kai Dang, Peng Wang, Shijie Wang, Jun Tang, et al. Qwen2. 5-vl technical report. *arXiv preprint arXiv:2502.13923*, 2025. 3

[3] Garrick Brazil, Abhinav Kumar, Julian Straub, Nikhila Ravi, Justin Johnson, and Georgia Gkioxari. Omni3d: A large benchmark and model for 3d object detection in the wild. In *Proceedings of the IEEE/CVF conference on computer vision and pattern recognition*, pages 13154–13164, 2023. 2

[4] Yang Cao, Zeng Yihan, Hang Xu, and Dan Xu. Coda: Collaborative novel box discovery and cross-modal alignment for open-vocabulary 3d object detection. *Advances in Neural Information Processing Systems*, 36:71862–71873, 2023. 2

[5] Yang Cao, Yihan Zeng, Hang Xu, and Dan Xu. Collaborative novel object discovery and box-guided cross-modal alignment for open-vocabulary 3d object detection. *IEEE Transactions on Pattern Analysis and Machine Intelligence*, 2025. 2

[6] Nicolas Carion, Francisco Massa, Gabriel Synnaeve, Nicolas Usunier, Alexander Kirillov, and Sergey Zagoruyko. End-to-end object detection with transformers. In *European conference on computer vision*, pages 213–229. Springer, 2020. 3

[7] Boyuan Chen, Zhuo Xu, Sean Kirmani, Brain Ichter, Dorsa Sadigh, Leonidas Guibas, and Fei Xia. Spatialvlm: Endowing vision-language models with spatial reasoning capabilities. In *Proceedings of the IEEE/CVF Conference on Computer Vision and Pattern Recognition*, pages 14455–14465, 2024. 3

[8] Jiahai Chen, Zhiyang Xu, Xichen Pan, Yushi Hu, Can Qin, Tom Goldstein, Lifu Huang, Tianyi Zhou, Saining Xie, Silvio Savarese, et al. Blip3-o: A family of fully open unified multimodal models-architecture, training and dataset. *arXiv preprint arXiv:2505.09568*, 2025. 3

[9] An-Chieh Cheng, Hongxu Yin, Yang Fu, Qiushan Guo, Ruihan Yang, Jan Kautz, Xiaolong Wang, and Sifei Liu. Spatial-rpt: Grounded spatial reasoning in vision-language models. *Advances in Neural Information Processing Systems*, 37:135062–135093, 2024. 3

[10] Angela Dai, Angel X. Chang, Manolis Savva, Maciej Halber, Thomas Funkhouser, and Matthias Nießner. Scannet: Richly-annotated 3d reconstructions of indoor scenes. In *Proc. Computer Vision and Pattern Recognition (CVPR), IEEE*, 2017. 2, 5, 6

[11] Navneet Dalal and Bill Triggs. Histograms of oriented gradients for human detection. In *2005 IEEE computer society conference on computer vision and pattern recognition (CVPR'05)*, pages 886–893. Ieee, 2005. 3

[12] Matt Deitke, Christopher Clark, Sangho Lee, Rohun Tripathi, Yue Yang, Jae Sung Park, Mohammadreza Salehi, Niklas Muennighoff, Kyle Lo, Luca Soldaini, et al. Molmo and pixmo: Open weights and open data for state-of-the-art vision-language models. In *Proceedings of the Computer Vision and Pattern Recognition Conference*, pages 91–104, 2025. 3

[13] Haiwen Diao, Mingxuan Li, Silei Wu, Linjun Dai, Xiaohua Wang, Hamming Deng, Lewei Lu, Dahua Lin, and Ziwei Liu. From pixels to words—towards native vision-language primitives at scale. *arXiv preprint arXiv:2510.14979*, 2025. 3

[14] Zhiwen Fan, Jian Zhang, Renjie Li, Junge Zhang, Runjin Chen, Hezhen Hu, Kevin Wang, Huaizhi Qu, Dilin Wang, Zhicheng Yan, et al. Vlm-3r: Vision-language models augmented with instruction-aligned 3d reconstruction. *arXiv preprint arXiv:2505.20279*, 2025. 3

[15] Pedro Felzenswalb, David McAllester, and Deva Ramanan. A discriminatively trained, multiscale, deformable part model. In *2008 IEEE conference on computer vision and pattern recognition*, pages 1–8. Ieee, 2008. 3

[16] Rao Fu, Jingyu Liu, Xilun Chen, Yixin Nie, and Wenhan Xiong. Scene-llm: Extending language model for 3d visual understanding and reasoning. *arXiv preprint arXiv:2403.11401*, 2024. 3

[17] Ross Girshick, Jeff Donahue, Trevor Darrell, and Jitendra Malik. Rich feature hierarchies for accurate object detection and semantic segmentation. In *Proceedings of the IEEE conference on computer vision and pattern recognition*, pages 580–587, 2014. 3

[18] Xiuye Gu, Tsung-Yi Lin, Weicheng Kuo, and Yin Cui. Open-vocabulary object detection via vision and language knowledge distillation. *arXiv preprint arXiv:2104.13921*, 2021. 3

[19] Kaiming He, Xiangyu Zhang, Shaoqing Ren, and Jian Sun. Spatial pyramid pooling in deep convolutional networks for visual recognition. *IEEE transactions on pattern analysis and machine intelligence*, 37(9):1904–1916, 2015. 3

[20] Wenbo Hu, Yining Hong, Yanjun Wang, Leison Gao, Zibu Wei, Xingcheng Yao, Nanyun Peng, Yonatan Bitton, Idan Szpektor, and Kai-Wei Chang. 3dllum-mem: Long-term spatial-temporal memory for embodied 3d large language model. *arXiv preprint arXiv:2505.22657*, 2025. 2, 3

[21] Rui Huang, Henry Zheng, Yan Wang, Zhuofan Xia, Marco Pavone, and Gao Huang. Training an open-vocabulary monocular 3d detection model without 3d data. *Advances in Neural Information Processing Systems*, 37:72145–72169, 2024. 2

[22] Ting Huang, Zeyu Zhang, and Hao Tang. 3d-r1: Enhancing reasoning in 3d vlms for unified scene understanding. *arXiv preprint arXiv:2507.23478*, 2025. 3

[23] Aaron Hurst, Adam Lerer, Adam P Goucher, Adam Perelman, Aditya Ramesh, Aidan Clark, AJ Ostrow, Akila Welihinda, Alan Hayes, Alec Radford, et al. Gpt-4o system card. *arXiv preprint arXiv:2410.21276*, 2024. 3

[24] Jin-Cheng Jhang, Tao Tu, Fu-En Wang, Ke Zhang, Min Sun, and Cheng-Hao Kuo. V-mind: Building versatile monocular indoor 3d detector with diverse 2d annotations. In *2025 IEEE/CVF Winter Conference on Applications of Computer Vision (WACV)*, pages 9577–9586. IEEE, 2025. 2

[25] Jianping Jiang, Weiyue Xiao, Zhengyu Lin, Huaizhong Zhang, Tianxiang Ren, Yang Gao, Zhiqian Lin, Zhongang Cai, Lei Yang, and Ziwei Liu. Solami: Social vision-language-action modeling for immersive interaction with 3d autonomous characters. In *Proceedings of the Computer Vision and Pattern Recognition Conference*, pages 26887–26898, 2025. 3

[26] Maksim Kolodiaznyi, Anna Vorontsova, Matvey Skripkin, Danila Rukhovich, and Anton Konushin. Unidet3d: Multi-dataset indoor 3d object detection. In *Proceedings of the AAAI Conference on Artificial Intelligence*, pages 4365–4373, 2025. 2

[27] Hei Law and Jia Deng. Cornernet: Detecting objects as paired keypoints. In *Proceedings of the European conference on computer vision (ECCV)*, pages 734–750, 2018. 3

[28] Junnan Li, Dongxu Li, Caiming Xiong, and Steven Hoi. Blip: Bootstrapping language-image pre-training for unified vision-language understanding and generation. In *International conference on machine learning*, pages 12888–12900. PMLR, 2022. 3

[29] Junnan Li, Dongxu Li, Silvio Savarese, and Steven Hoi. Blip-2: Bootstrapping language-image pre-training with frozen image encoders and large language models. In *International conference on machine learning*, pages 19730–19742. PMLR, 2023. 3

[30] Liunian Harold Li, Pengchuan Zhang, Haotian Zhang, Jianwei Yang, Chunyuan Li, Yiwu Zhong, Lijuan Wang, Lu Yuan, Lei Zhang, Jenq-Neng Hwang, et al. Grounded language-image pre-training. In *Proceedings of the IEEE/CVF conference on computer vision and pattern recognition*, pages 10965–10975, 2022. 3

[31] Zhuoling Li, Xiaogang Xu, Ser-Nam Lim, and Hengshuang Zhao. Towards unified 3d object detection via algorithm and data unification. *IEEE Transactions on Pattern Analysis and Machine Intelligence*, 2025. 2

[32] Tsung-Yi Lin, Priya Goyal, Ross Girshick, Kaiming He, and Piotr Dollár. Focal loss for dense object detection. In *Proceedings of the IEEE international conference on computer vision*, pages 2980–2988, 2017. 3

[33] Haotian Liu, Chunyuan Li, Qingyang Wu, and Yong Jae Lee. Visual instruction tuning. *Advances in neural information processing systems*, 36:34892–34916, 2023. 3

[34] Shilong Liu, Zhaoyang Zeng, Tianhe Ren, Feng Li, Hao Zhang, Jie Yang, Qing Jiang, Chunyuan Li, Jianwei Yang, Hang Su, et al. Grounding dino: Marrying dino with grounded pre-training for open-set object detection. In *European conference on computer vision*, pages 38–55. Springer, 2024. 2, 3

[35] Wei Liu, Dragomir Anguelov, Dumitru Erhan, Christian Szegedy, Scott Reed, Cheng-Yang Fu, and Alexander C Berg. Ssd: Single shot multibox detector. In *European conference on computer vision*, pages 21–37. Springer, 2016. 3

[36] Yuheng Lu, Chenfeng Xu, Xiaobao Wei, Xiaodong Xie, Masayoshi Tomizuka, Kurt Keutzer, and Shanghang Zhang. Open-vocabulary 3d detection via image-level class and de-biased cross-modal contrastive learning. *arXiv preprint arXiv:2207.01987*, 2022. 2

[37] Yuheng Lu, Chenfeng Xu, Xiaobao Wei, Xiaodong Xie, Masayoshi Tomizuka, Kurt Keutzer, and Shanghang Zhang. Open-vocabulary point-cloud object detection without 3d annotation. In *Proceedings of the IEEE/CVF conference on computer vision and pattern recognition*, pages 1190–1199, 2023. 2

[38] Wufei Ma, Luoxin Ye, Celso M de Melo, Alan Yuille, and Jieneng Chen. Spatialllm: A compound 3d-informed design towards spatially-intelligent large multimodal models. In *Proceedings of the Computer Vision and Pattern Recognition Conference*, pages 17249–17260, 2025. 3

[39] Yongsen Mao, Junhao Zhong, Chuan Fang, Jia Zheng, Rui Tang, Hao Zhu, Ping Tan, and Zihan Zhou. Spatialllm: Training large language models for structured indoor modeling. *arXiv preprint arXiv:2506.07491*, 2025. 3, 5, 1

[40] Xingyu Peng, Yan Bai, Chen Gao, Lirong Yang, Fei Xia, Beipeng Mu, Xiaofei Wang, and Si Liu. Global-local collaborative inference with llm for lidar-based open-vocabulary detection. In *European Conference on Computer Vision*, pages 367–384. Springer, 2024. 2

[41] Zekun Qi, Runpei Dong, Shaochen Zhang, Haoran Geng, Chunrui Han, Zheng Ge, Li Yi, and Kaisheng Ma. Shapellm: Universal 3d object understanding for embodied interaction. In *European Conference on Computer Vision*, pages 214–238. Springer, 2024. 3

[42] Alec Radford, Jong Wook Kim, Chris Hallacy, Aditya Ramesh, Gabriel Goh, Sandhini Agarwal, Girish Sastry, Amanda Askell, Pamela Mishkin, Jack Clark, et al. Learning transferable visual models from natural language supervision. In *International conference on machine learning*, pages 8748–8763. PMLR, 2021. 3, 7

[43] Joseph Redmon, Santosh Divvala, Ross Girshick, and Ali Farhadi. You only look once: Unified, real-time object detection. In *Proceedings of the IEEE conference on computer vision and pattern recognition*, pages 779–788, 2016. 3

[44] Shaoqing Ren, Kaiming He, Ross Girshick, and Jian Sun. Faster r-cnn: Towards real-time object detection with region proposal networks. *Advances in neural information processing systems*, 28, 2015. 3

[45] Tianhe Ren, Shilong Liu, Ailing Zeng, Jing Lin, Kun-chang Li, He Cao, Jiayu Chen, Xinyu Huang, Yukang Chen, Feng Yan, Zhaoyang Zeng, Hao Zhang, Feng Li, Jie Yang, Hongyang Li, Qing Jiang, and Lei Zhang. Grounded sam: Assembling open-world models for diverse visual tasks, 2024. 5

[46] Yichao Shen, Zigang Geng, Yuhui Yuan, Yutong Lin, Ze Liu, Chunyu Wang, Han Hu, Nanning Zheng, and Baining Guo. V-detr: Detr with vertex relative position encoding for 3d object detection. *arXiv preprint arXiv:2308.04409*, 2023. 2

[47] Hugo Touvron, Thibaut Lavril, Gautier Izacard, Xavier Martinet, Marie-Anne Lachaux, Timothée Lacroix, Baptiste Rozière, Naman Goyal, Eric Hambro, Faisal Azhar, et al. Llama: Open and efficient foundation language models. *arXiv preprint arXiv:2302.13971*, 2023. 3, 4, 7

[48] Paul Viola and Michael Jones. Rapid object detection using a boosted cascade of simple features. In *Proceedings of the 2001 IEEE computer society conference on computer vision*

and pattern recognition. CVPR 2001, pages I–I. Ieee, 2001. 3

[49] Qianqian Wang, Yifei Zhang, Aleksander Holynski, Alexei A Efros, and Angjoo Kanazawa. Continuous 3d perception model with persistent state. In *Proceedings of the Computer Vision and Pattern Recognition Conference*, pages 10510–10522, 2025. 5, 6

[50] Diankun Wu, Fangfu Liu, Yi-Hsin Hung, and Yueqi Duan. Spatial-mllm: Boosting mllm capabilities in visual-based spatial intelligence. *arXiv preprint arXiv:2505.23747*, 2025. 3

[51] Xiaoyang Wu, Daniel DeTone, Duncan Frost, Tianwei Shen, Chris Xie, Nan Yang, Jakob Engel, Richard Newcombe, Hengshuang Zhao, and Julian Straub. Sonata: Self-supervised learning of reliable point representations. In *Proceedings of the Computer Vision and Pattern Recognition Conference*, pages 22193–22204, 2025. 3, 4, 1

[52] Jinheng Xie, Weijia Mao, Zechen Bai, David Junhao Zhang, Weihao Wang, Kevin Qinghong Lin, Yuchao Gu, Zhijie Chen, Zhenheng Yang, and Mike Zheng Shou. Show-o: One single transformer to unify multimodal understanding and generation. *arXiv preprint arXiv:2408.12528*, 2024. 3

[53] Jin Xu, Zhifang Guo, Hangrui Hu, Yunfei Chu, Xiong Wang, Jinzheng He, Yuxuan Wang, Xian Shi, Ting He, Xinfa Zhu, et al. Qwen3-omni technical report. *arXiv preprint arXiv:2509.17765*, 2025. 3

[54] Runsen Xu, Xiaolong Wang, Tai Wang, Yilun Chen, Jiangmiao Pang, and Dahu Lin. Pointllm: Empowering large language models to understand point clouds. In *European Conference on Computer Vision*, pages 131–147. Springer, 2024. 3

[55] Runsen Xu, Weiyao Wang, Hao Tang, Xingyu Chen, Xiaodong Wang, Fu-Jen Chu, Dahua Lin, Matt Feiszli, and Kevin J Liang. Multi-spatialmllm: Multi-frame spatial understanding with multi-modal large language models. *arXiv preprint arXiv:2505.17015*, 2025. 3

[56] Yuncong Yang, Han Yang, Jiachen Zhou, Peihao Chen, Hongxin Zhang, Yilun Du, and Chuang Gan. 3d-mem: 3d scene memory for embodied exploration and reasoning. In *Proceedings of the Computer Vision and Pattern Recognition Conference*, pages 17294–17303, 2025. 3

[57] Jin Yao, Hao Gu, Xuweiyi Chen, Jiayun Wang, and Zezhou Cheng. Open vocabulary monocular 3d object detection. *arXiv preprint arXiv:2411.16833*, 2024. 2

[58] Chandan Yeshwanth, Yueh-Cheng Liu, Matthias Nießner, and Angela Dai. Scannet++: A high-fidelity dataset of 3d indoor scenes. In *Proceedings of the International Conference on Computer Vision (ICCV)*, 2023. 2, 5, 6, 7, 8

[59] Yuhang Zang, Wei Li, Kaiyang Zhou, Chen Huang, and Chen Change Loy. Open-vocabulary detr with conditional matching. In *European conference on computer vision*, pages 106–122. Springer, 2022. 3

[60] Hanxue Zhang, Haoran Jiang, Qingsong Yao, Yanan Sun, Renrui Zhang, Hao Zhao, Hongyang Li, Hongzi Zhu, and Zetong Yang. Detect anything 3d in the wild. *arXiv preprint arXiv:2504.07958*, 2025. 2

[61] Duo Zheng, Shijia Huang, Yanyang Li, and Liwei Wang. Learning from videos for 3d world: Enhancing mllms with 3d vision geometry priors. *arXiv preprint arXiv:2505.24625*, 2025. 3

[62] Chenming Zhu, Tai Wang, Wenwei Zhang, Jiangmiao Pang, and Xihui Liu. Llava-3d: A simple yet effective pathway to empowering lmms with 3d-awareness. *arXiv preprint arXiv:2409.18125*, 2024. 3

[63] Ziyu Zhu, Xilin Wang, Yixuan Li, Zhuofan Zhang, Xiaojian Ma, Yixin Chen, Baoxiong Jia, Wei Liang, Qian Yu, Zhi-dong Deng, et al. Move to understand a 3d scene: Bridging visual grounding and exploration for efficient and versatile embodied navigation. In *Proceedings of the IEEE/CVF International Conference on Computer Vision*, pages 8120–8132, 2025. 2

[64] Xueyan Zou, Yuchen Song, Ri-Zhao Qiu, Xuanbin Peng, Jianglong Ye, Sifei Liu, and Xiaolong Wang. 3d-spatial multimodal memory. In *The Thirteenth International Conference on Learning Representations*, 2025. 3

OnlineSI: Taming Large Language Model for Online 3D Understanding and Grounding

Supplementary Material

7. More Implementation Details

7.1. Spatial Memory Management

In Sec. 4.2, to maintain a fixed size for \mathbf{M}_t and prevent rapid forgetting, we automatically adjust the fusion ratio based on timestep t . Here we formulate the fusion process. Following the notations in Sec. 4.2, we reformulate Eq. 2 as:

$$\mathbf{P}_t = \text{Sample}(\text{Concat}(\mathbf{P}_{t-1}, \text{Sample}(\mathbf{X}'_t, \alpha_t)), \beta_t), \mathbf{P}_0 = \emptyset, \quad (4)$$

$$\mathbf{S}_t = \text{Sample}(\text{Concat}(\mathbf{S}_{t-1}, \text{Sample}(\mathbf{Y}_t, \alpha_t)), \beta_t), \mathbf{S}_0 = \emptyset, \quad (5)$$

Here $\text{Sample}(\mathbf{A}, \alpha)$ means sampling \mathbf{A} at ratio α , $\text{Concat}(\cdot, \cdot)$ means concatenating two inputs. Assume we set the maximum memory limit to accommodate N frames of input, then we have:

$$\alpha_t = \begin{cases} 1, & t \leq N \\ \frac{N}{t-1}, & t > N \end{cases} \quad (6)$$

$$\beta_t = \begin{cases} 1, & t \leq N \\ \frac{t-1}{t}, & t > N \end{cases} \quad (7)$$

It's easy to verify that this ensures a fixed upper limit for memory size, and that each input frame occupies the same proportion in memory.

7.2. Point Cloud Encoder and Semantic Encoder

Here we further elaborate on the design of the semantic encoder. As shown in Fig. 6, the point cloud encoder follows the design in Sonate [51]. For the semantic encoder, in the embedding layer we first leverage Llama's tokenizer to divide the semantic label into tokens of variable length, and then take the average of these token features as the corresponding text feature. We then use only the pooling operations to aggregate these per-point features into semantic feature patches, and fine-tune only the last linear projection layer for the fusion of different representations.

8. More Experiment Details

Listing 1. Prompt of the LLM Backbone

```
<|point_start|><|point_pad|><|point_end|>Detect
  chair, table, computer, curtain, sink, bed,
  bookcase, sofa, toilet, tub. The reference
  code is as followed:
@dataclass
```

```
class Wall:
    ax: int
    ay: int
    az: int
    bx: int
    by: int
    bz: int
    height: int
    thickness: int

@dataclass
class Door:
    wall_id: str
    position_x: int
    position_y: int
    position_z: int
    width: int
    height: int

@dataclass
class Window:
    wall_id: str
    position_x: int
    position_y: int
    position_z: int
    width: int
    height: int

@dataclass
class Bbox:
    class: str
    position_x: int
    position_y: int
    position_z: int
    angle_z: int
    scale_x: int
    scale_y: int
    scale_z: int
```

Experiment Settings Some room types in ScanNet and ScanNet++ are not suitable for SpatialLM [39] (SpatialLM lacks relevant prior knowledge). In our experiments, we choose a subset of room types, as well as 10 object categories for training and validation to minimize the distribution shift of data, as shown in Tab. 4. Following SpatialLM, the prompt we use for the LLM backbone is demonstrated in Lst. 1. We replace `<|point_pad|>` with the spatial memory tokens for inference.

Baseline Settings Here we illustrate some implementation details of the baselines. **1.** In SpatialLM-Merge, for each newly predicted bounding box, we will match it against existing bounding boxes of the same type using the Hungarian algorithm. If the IoU of the matched bounding box is greater than 0.25, the matched bounding box will be updated as the new bounding box. **2.** In the two ground-truth

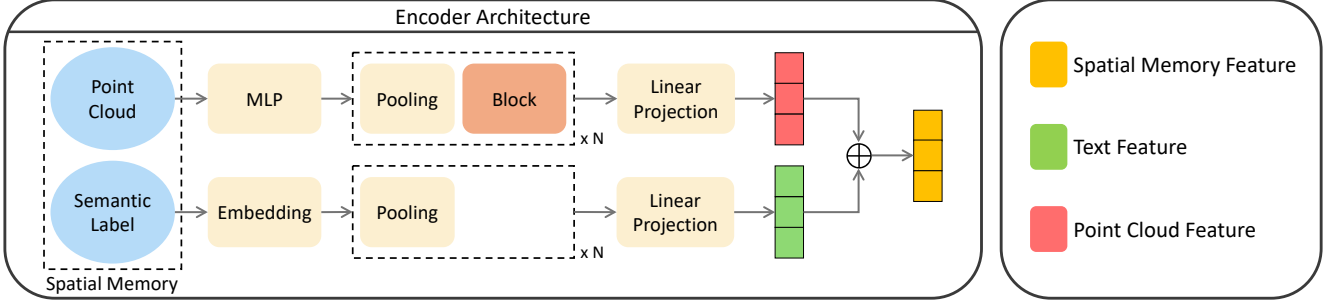


Figure 6. **Point Cloud Encoder and Semantic Encoder.** For the semantic encoder, we first transform the semantic label into text features through embedding operations, and then obtain semantic feature patches through pooling operations with the same structure as Sonata.

Room Types		‘office’, ‘kitchen’, ‘bathroom’, ‘apartment’, ‘living room / lounge’, ‘bedroom / hotel’
Object Categories		‘chair’, ‘table’, ‘computer’, ‘curtain’, ‘sink’, ‘bed’, ‘bookcase’, ‘sofa’, ‘toilet’, ‘tub’

Table 4. **Experiment Settings.** We select 6 room types and 10 object categories for training and validation to minimize distribution shift.

baselines, we project the depth map to 3D as the ground-truth point cloud of each frame. In addition, for the training of all baselines we use ground-truth point clouds and semantic labels. The difference between lower-bound baselines and ground-truth baselines is whether the ground-truth data is available during inference.